Characterization of a miniaturized ultrasound transducer customized for oral health applications

Baiyan Qi[1], Ali Hariri[2*], Reza Khazaeinezhad[2], Lei Fu[3], and Jesse V. Jokerst[1,3,4*]

1 Materials Science and Engineering Program
University of California San Diego, La Jolla, California 92093, USA
2 StyloSonic LLC
Lake Forest, California 92630, USA
3 Department of NanoEngineering
University of California San Diego, La Jolla, California 92093, USA
4 Department of Radiology
University of California San Diego, La Jolla, California 92093, USA
*E-mail: jjokerst@eng.ucsd.edu, ali@stylosonic.com

Abstract

Periodontitis affects nearly 50% of Americans. Conventional clinical assessment based on periodontal probing remains the gold standard despite being operator-dependent, time-consuming, and often painful. In contrast, ultrasound imaging is non-invasive, portable, low-cost, and free of ionizing radiation. Unfortunately, most conventional ultrasound transducers can only access anterior teeth due to the size of the imaging equipment. Here, we characterized a novel and customized periodontal ultrasound transducer SS-19-128 that can examine the entire human mouth. The transducer is 1.8 cm width by 1 cm height, including 128 channels with a center frequency of 19 MHz. The axial and lateral spatial resolution at 5.5 mm depth is 102.1 μm and 142.9 μm, respectively. The penetration depth in tissue mimicking phantom is over 31 mm. Imaging was performed on 3 human subjects, and statistical analysis on swine jaws indicated a high agreement with the gold standard.

1. Introduction

Nearly 50% of Americans have periodontitis[1] resulting in pain, tooth loss[2,3], reduced quality of life and even systemic effects like cardiovascular disease, but tools to diagnose/monitor periodontitis have major limitations. Clinical assessment (by periodontal examination) and radiography are currently the standard of care but suffer from major limitations. Radiography offers excellent sensitivity to hard tissue (bone, enamel, etc.) but cannot discriminate between healthy and diseased gingiva or map disease within soft tissue; radiography also has a small but non-negligible dose of ionizing radiation. Periodontal examination provides critical information such as periodontal probing depths (PPD; current periodontal health) and clinical attachment loss (CAL). PPD, CAL, and other clinical parameters form the basis of periodontal diagnosis. However, periodontal examination is time-consuming for the provider and painful for the patient and suffers from large errors—inter-operator variation in probing can be >40%. Moreover, clinical assessment and radiographic examination may not capture all clinical information (e.g., gingival thickness and inflammation).

To solve these major limitations, we[4,5] and others[6–9] have shown that ultrasound and photoacoustic imaging have major value in oral health. The most relevant works have demonstrated the visualization of anatomical features including the alveolar bone crest (ABC), cementoenamel junction (CEJ), gingival thickness (GT), edentulous crestal bone, greater palatine foramen, lingual nerve, and oral mucosa in healthy humans, ex vivo swine jaws, and cadavers[8,10–14]. Machine and deep learning have also been used to automate image analysis[9,15,16]. Other work is improving transducer design and form factor via improved hardware and coupling materials[17,18].However, further clinical translation and validation of this imaging technology are limited by the size of current transducers—most existing transducers are simply too bulky to access molars and pre-molars and can only image incisors and canines. While many compact and endoscopic ultrasound transducers are available commercially, none offer the high frequency needed to resolve small dental feature sizes.

To resolve the limited access to deeper teeth of the conventional bulky transducers, we describe here a customized 128-element, 19-MHz transducer for periodontal imaging. The form factor ensures access to the entire oral cavity including all molars. Here, we first evaluated the device's axial and lateral resolution and imaging depth. We then used it to identify landmarks in the oral anatomy in both humans and cadaver swine. We further used the intraoral scanner to measure the gingival thickness and compared image-based metrics to gold standard techniques. The results suggest that this device has value in assessing disease in the mouth.

2. Materials and methods

Equipment

This work used a customized transducer (SS-19-128; StyloSonic (Lake Forest, CA)). This customized periodontal transducer has a 128-element linear array with a center frequency of 19 MHz and an average -6 dB bandwidth of 48.9%. The length of the ultrasound active area is 10.24 mm with element pitch size of 78 μm. The transducer is housed inside a handpiece (1.8 cm x 1 cm) to access the entire oral cavity. The transducer has a side-facing view within the housing to ensure proper positioning with the gingiva and tooth surface.

The transducer was connected to a data acquisition (DAQ) system (Vantage 256, Verasonics, Inc.) via a UTA 260D adapter. The DAQ provided a 5.6-V power supply and controlled electrical excitement time delay. The DAQ sampled all radiofrequency data and processed ultrasound images. This system supports frequency range from 2 to 42 MHz, 14-bit A/D converters with programmable sample rate up to 62.5 MHz, and can image up to 100,000 frames/second. A CL15-7 transducer from Philips was used for comparison.

Preparation of Tissue-Mimicking Phantom

A polyacrylamide (PAA)-based tissue mimicking phantom was used in this study[19]. The phantom contained an array of light-wall polytetrafluoroethylene tubes (Component Supply Co., Sparta, TN) at depths of 5−35 mm. Tubes were filled with water. PAA phantoms were fabricated from a 400 mL batch of solution using a final recipe of 12% w/v acrylamide, 0.08% w/v APS, 0.2% v/v TEMED, 0.7 mg/mL TiO_2, 0.00225% v/v India ink, and 6 mg/mL glass beads. Phantoms took approximately five min to solidify and were allowed to cure for 1 h, with a maximum surface temperature of 46 °C as measured by an infrared thermometer.

Swine Studies

Swine jaws were purchased from the local butcher and sliced with a bandsaw to size. They were immobilized under water for ultrasound coupling for imaging. Values of gingival thickness were measured by SS-19-128 imaging and a 28-gauge needle with calipers (gold standard method)[20,21]. The gingival thickness measurement point was defined as 2-mm below the gingival margin. In the ultrasound imaging method, the gingival thickness was obtained by measuring the distance between the gingival surface and the tooth surface. In the gold standard method, the needle was inserted into the gingiva perpendicularly until contact with the tooth. A line was marked on the needle, and the distance between the marked line and the tip of the needle was measured with a 0.1-mm precision caliper.

Human Subjects Imaging

Three healthy male adults (between 25-40 years old) with good oral hygiene were enrolled. The study with human subjects was approved by the IRB at University of California – San Diego (170912) and was conducted according to the ethical standards set forth by the IRB and the Helsinki Declaration of 1975. All subjects gave informed

consent. The transducer was enclosed within a layer of parafilm with a thin amount of gel between the transducer surface and the parafilm. Coupling gel was also placed on the exterior of the parafilm wrapped device to couple it to the teeth.

Imaging Procedures

Three different modes of beamforming were used to process ultrasound images: no flash angle, flash angles, and wide beam[22]. In no flash angle mode, all channels of the transducer were excited spontaneously to generate only one plane wave with no beam tilting, and B-mode image was reconstructed from the ultrasound pulse-echo signal[23]. In flash angles mode (also known as coherent compounding method), a time delay between channels was applied by the DAQ system[24]. Seven plane waves with different tilting angles were generated in a row, and one image frame was reconstructed by averaging the images obtained with all tilted plane waves. In wide beam mode, channels were divided into many subgroups and in each ultrasound image frame, all subgroups swiped from one side to the end along the transducer array[23]. The reconstruction process was to compensate the phase differences and then add up the pulse-echo signals from all channels.

Statistical analysis

Bland-Altman plot and Pearson correlation comparing ultrasound imaging method and needle measurement on 12 swine teeth were analyzed by GraphPad Prism 9 to characterize the accuracy of gingival thickness measurement with SS-19-128.

3. Results and Discussion

Our goal here was to use a custom-built 1.8 cm by 1 cm for oral imaging. We first measured the axial and lateral resolution as well as penetration depth (imaging depth). We enrolled three healthy subjects for ultrasound imaging of periodontal structures and could successfully access all molars including #32. We used the transducer to measure the gingival thickness on 12 swine teeth.

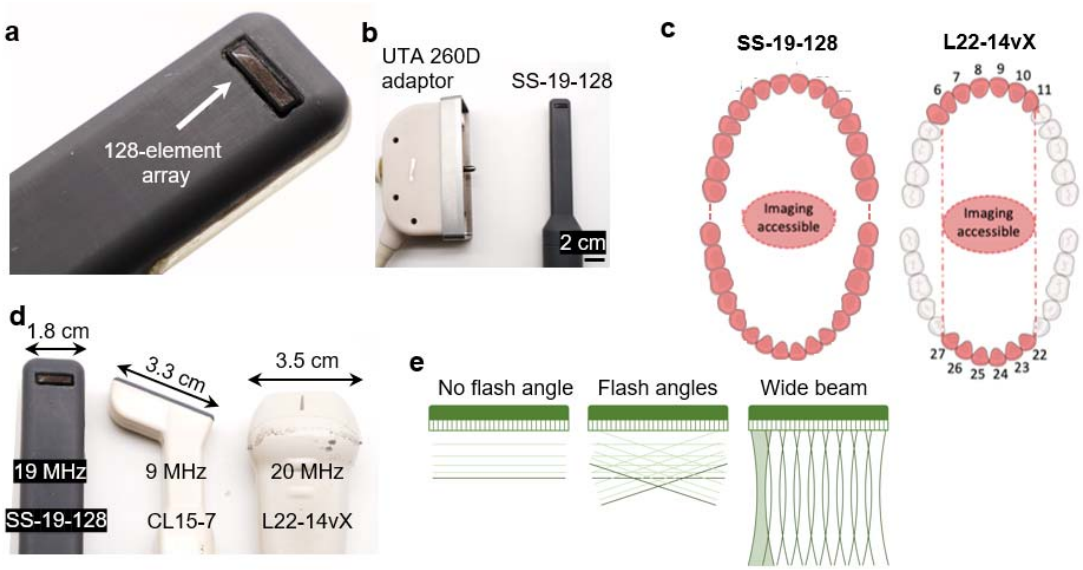

Figure 1. Overview of SS-19-128 and periodontal imaging. (a) Photograph of the SS-19-128 transducer showing the 128-channel array integrated into a 3D-printed handpiece for intraoral imaging. (b) Lower magnification photograph of the connector used for the DAQ and the entire handpiece. (c) Comparison of accessible imaging range between SS-19-128 and L22-14vX due to size restrictions. (d) Comparison of ultrasound transducers with utility in periodontal imaging. The head width of SS-19-128 is decreased by ~two-fold versus CL15-7 and L22-14vX. (e) Illustration of the three beamforming modes used here for ultrasound B-mode imaging. No flash angle mode has only one plane wave; flash angles mode has several tilted plane waves for coherent compounding; and wide beam mode has beams in subgroups sweeping along the transducer array.

System setup and periodontal anatomy. The transducer has dimensions suitable for accessing the entire oral cavity (**Fig. 1a**) and was fitted with universal transducer adapter suitable for interfacing with the DAQ (**Fig. 1b**). Importantly, this compact form factor and side-facing view can image all 32 adult human teeth. The gums restrict the movement and positioning of larger transducers or transducers with front-facing designs (**Fig. 1c**). More specifically, the width of SS-19-128 was 1.83- and 1.94 times smaller compared with the representative transducers with potential utility in intraoral imaging (CL15-7 and L22-14vX, respectively; (**Fig. 1d**). The center frequency is 19

MHz, which is comparable to the 20 MHz L22-vX and two times higher than the 9 MHz CL15-7. A more complete comparison to similar transducers is given in **Table 1**.

Table 1. Comparison of SS-19-128 with other transducers used for periodontal imaging. NR: not reported.

Manufacturer –Transducer	**StyloSonic –SS-19-128**	**Zonare/Mindray – L25-8**	**VisualSonics – UHF70**	**Olympus – V116**	**Vinno – X10-23L**	**Analogic – L40-8/12**
Element number	128	NR	NR	1	128	128
Frequency	19 MHz	25 MHz	70 MHz	20 MHz	23 MHz	20 MHz
Side or Forward Facing	Side	Side	Forward	Right microdot	Forward	Forward
Size	Thickness 10 mm; width 18 mm	Maximal transducer thickness, width and length is 15, 16.2, and 30 mm	~ 1 x 2 x 10 cm	6.4 mm by 9.7 mm	NR	13mm × 4mm
Axial Res (µm)	102.1 µm	64 µm	30 µm	NR	NR	NR
Lateral Res (µm)	142.9	192	65	NA	NR	NR
Field of View	1	1.7	0.97	NA	NR	NR
Penetration (mm)	>30	15	10	NR	NR	16
Ref		[25]	[10]	[13]	[26]	[9]

Resolution and penetration depth performance

Higher frequency transducers lead to better resolution but lower penetration depth. Fortunately, dental ultrasound rarely requires deep imaging, i.e., ~ 1 cm max to the tooth surface. However, the size of the oral features (CEJ, gingival thickness, etc.) are often on the sub-millimeter scale or else high-precision measurements are needed[27]. Thus, there is value in transducers with higher frequencies because they offer better resolution.

We placed two 30-µm nichrome wires in water and held them 5.5 and 13.5 mm from the surface of the transducer (**Fig. 2a**). We compared three different beamforming modes: no flash, flash angle, and wide beam (**Fig. 1e** and **Fig. 2b**)[22]. The resolution was characterized by applying the line spread function[28]. The axial (**Fig. 2c**) and lateral (**Fig. 2d**) resolution were characterized under all three beamforming modes. Axial resolution is mostly dependent on center frequency and the pulse cycle number[29]. These two parameters are set as the same, and thus the axial resolution was similar in all three modes. Lateral resolution is related to beamwidth, which is different between the three modes.

The axial resolutions of no flash and flash angles modes were both 102.1 µm, which was 9.2% higher than the wide beam mode (112.5 µm). It is known[30] that axial resolution = spatial pulse length (SPL)/2, and SPL is proportional to wavelength and

pulse cycle number[29]. The wavelength and pulse cycle number were the same in these three modes and thus the values should be identical but there was actually a ~10% difference perhaps due to subtle differences in the positioning of the phantom relative to the transducer.

The lateral resolution of the wire 5.5 mm from the transducer was 142.9 μm in flash angle mode—this is 36.4% lower than no flash mode (224.6 μm) and 58.8% lower than wide beam mode (347.1 μm). Under flash angle mode, the artifacts in the lateral direction were compressed by averaging radiofrequency signals from plane waves with seven tilting angles[31]. Of course, our goal here was low resolution for the small oral features, and thus flash angle beamforming was used for subsequent work.

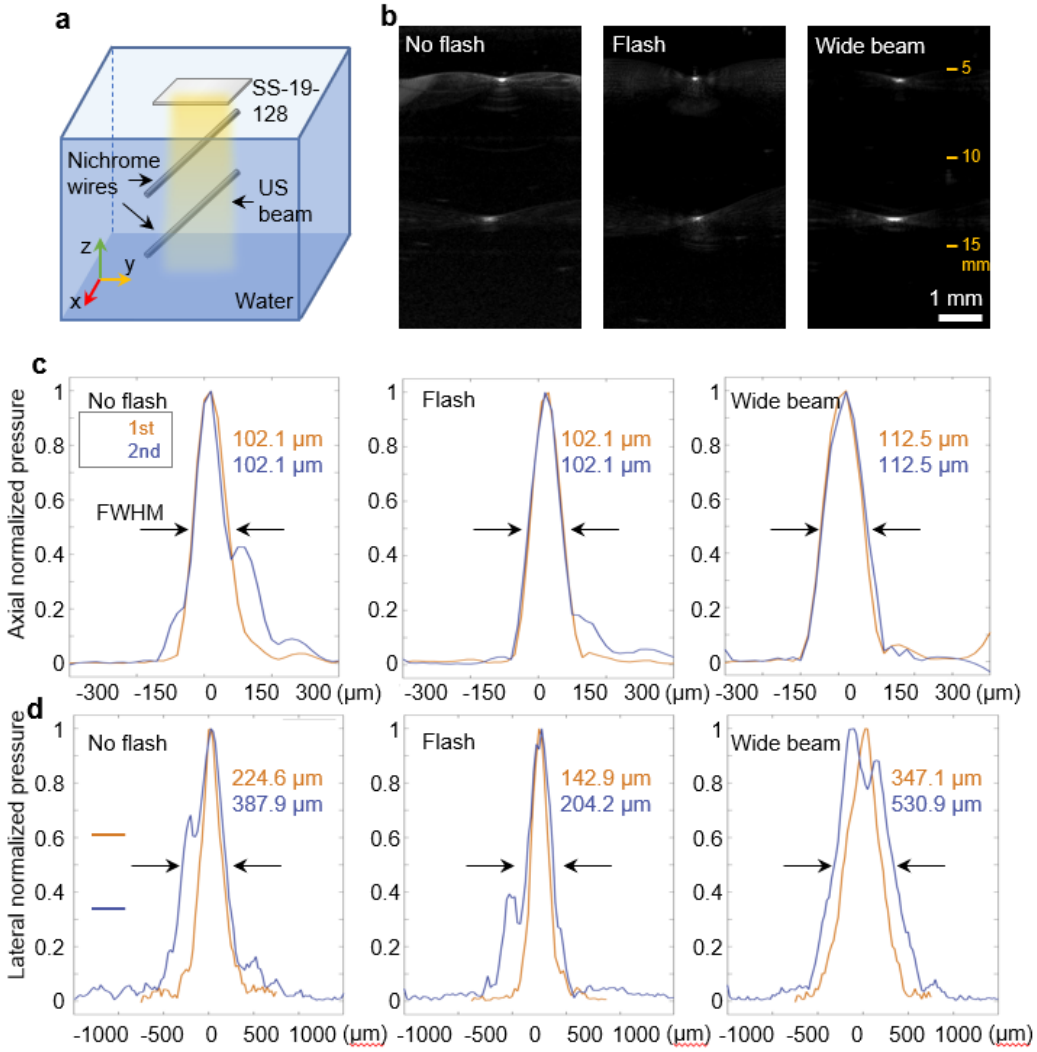

Figure 2. Spatial resolution characterization. (a) Schematics of the characterization system: Two ultra-thin nichrome wires are fixed in water 5.5 and 13.5 mm beneath the transducer. (b) Ultrasound imaging with three beamforming modes. (c) Axial and (d) lateral resolution characterization at two depths.

The penetration of acoustic pressure waves decreases with increasing frequency due to faster attenuation[32]. Here, we tested the penetration depth of the intraoral transducer a tissue-mimicking phantom with polytetrafluoroethylene tubes embedded at different depths (**Fig. 3a**). The signal-to-noise ratio (SNR) of the 30-mm-deep tubes were 19 dB, 22 dB, and 21 dB under no flash, flash angles, and wide beam modes, respectively, (**Fig. 3b**). The results show that SS-19-128 can easily evaluate the entire gingiva (median gingival thickness =1.1 mm[33]). The SNR vs depth under three beamforming modes is further quantitated in **Fig. 3c**.

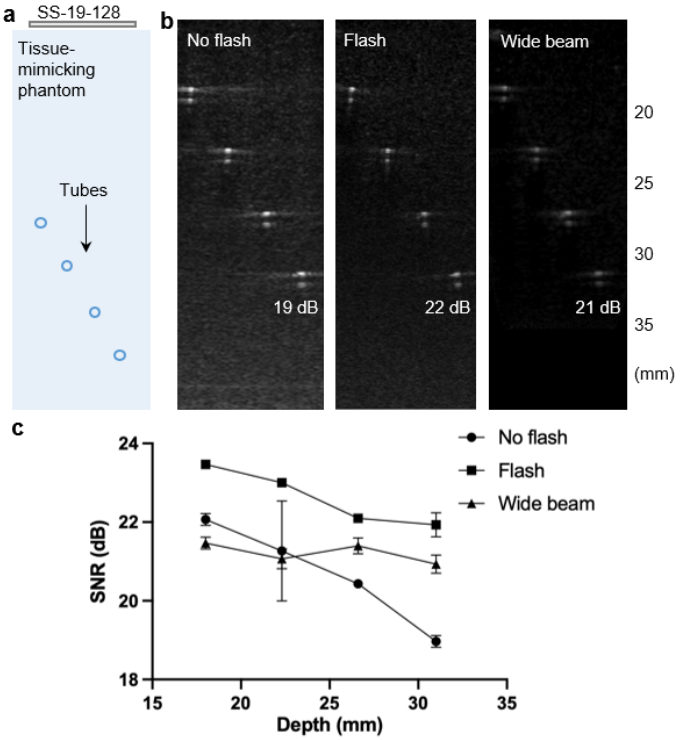

Figure 3. Contrast of ultrasound imaging in tissue-mimicking phantom. (a) Schematics of the phantom. Four light-wall polytetrafluoroethylene tubes are buried at different depth in the phantom to reflect ultrasound signals. (b) ultrasound imaging with three beamforming modes. (c) SNR vs depth curve.

Periodontal imaging on human subjects

This human subjects work enrolled three volunteers. We imaged tooth #30 and #32 of subject #1, #8 and #19 of subject #2, and #5 and #14 of subject #3 with SS-19-128. Imaging of the last lower right molar (#32) was achieved (**Fig. 4**). The results indicated that the device has value in imaging molars due to its form factor. We also compared human tooth #8 images obtained by SS-19-128 and conventional CL15-7 transducer (Fig. S). Thanks to the 2.1 times higher frequency, SS-19-128 had a resolution that was enhanced 2-fold relative to CL15-7 (axial resolution = 200 μm).

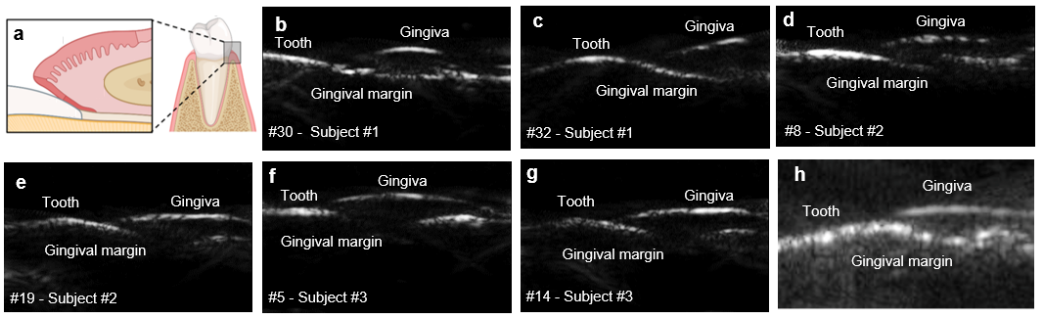

Figure 4. Imaging on human subjects. a) Schematic of the area imaged in panels b-h. Panels b-g were imaged with SS-18-128 across three human subjects including #32. Panel h is a control scan using CL15-7 (9 MHz).

Gingival Thickness Measurement

The values of gingival thickness were measured 2 mm apical to the gingival margin[33] with ultrasound (**Fig. 5a**) and with a needle. The gingival thickness values ranged from 1.0 to 1.6 mm in both methods. Bland-Altman plot (**Fig. 5b**) shows that the bias was -0.15 mm, indicating that needle measurements gave slightly lower values. Pearson correlation (**Fig. 5c**) shows that the correlation coefficient r = 0.9235 (P<0.0001), indicating a high correlation agreement between two measurements.

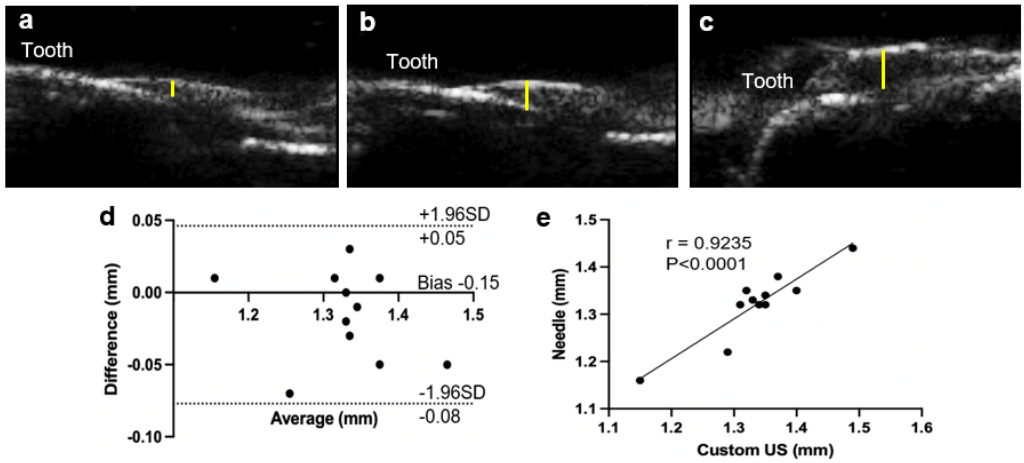

Figure 5. Gingival thickness measurement on swine jaws and statistical analysis. Examples of swine teeth ultrasound images collected with SS-19-128 for gingival thickness including small (a), medium (b), and larger gingival thickness (c); yellow line indicates approximate area of measurement. (d) Bland-Altman plot comparing ultrasound imaging and needle measurements, indicating a -0.15 mm bias between two measurements. (c) Pearson correlation between ultrasound imaging and needle measurement. Correlation coefficient r = 0.9235 (P<0.0001) showing a high correlation relationship between two measurements. Yellow line in a-c indicates the gingival thickness.

This study reports ultrasound imaging by SS-19-128 measuring gingival thickness. This minimized SS-19-128 offers access to the entire oral cavity for assessment of

periodontal disease. The transducer can image important anatomical landmarks in real time. The metrics measured with this device correlate nicely to gold standard metrics.

Future work will improve the excitation voltage and handpiece design. The highest voltage that can be applied to SS-19-128 is 5.6 V, which has an order of magnitude less than conventional transducers (30 V-50 V). Additional engineering of the handpiece will work to future reduce the form factor and increase ergonomics. Clinically, we will work to enroll a more representative cohort including subjects with periodontal disease and extract metrics of periodontal disease as we described previously with a larger 40-MHz transducer from an alternative commercial source.

4. Conclusion

This study reports a custom transducer to full mouth imaging of the periodontium. The transducer can easily access all human teeth including the molars. The images on human subjects are comparable to the conventional bulky transducer. The values of gingival thickness by imaging strongly correlated with clinical methods. In future works, we will further improve the image quality of the transducer, expand the measurement to a larger population, and demonstrate utility in diseased subjects.

Conflict of interests

R.K., A.H., and J.V.J. are co-founders of StyloSonic.

Acknowledgements

A.H. and R.K. acknowledge federal funding from NIH under R43 DE031196. J.V.J acknowledges NIH funding under R21 DE029025 and UL1 TR001442. Some figures were prepared under a license with BioRender.

References

1. Eke, P. I., Dye, B. A., Wei, L., Thornton-Evans, G. O. & Genco, R. J. Prevalence of Periodontitis in Adults in the United States: 2009 and 2010. Journal of Dental Research 91, 914-920, doi:10.1177/0022034512457373 (2012).
2. Inglehart, M. R. & Bagramian, R. Oral health-related quality of life. (Quintessence Pub., 2002).
3. Brennan, D. S., Spencer, A. J. & Roberts-Thomson, K. F. Tooth loss, chewing ability and quality of life. Quality of Life Research 17, 227-235 (2008).
4. Mozaffarzadeh, Moein, et al. ‘Motion-compensated noninvasive periodontal health monitoring using handheld and motor-based photoacoustic-ultrasound imaging systems.’ Biomedical Optics Express 12.3 (2021): 1543-1558.
5. Lin, C. Y., et al. ‘Photoacoustic imaging for noninvasive periodontal probing depth measurements.’ Journal of dental research 97.1 (2018): 23-30.

6. Le, Lawrence H., et al. ‘Ultrasound for Periodontal Imaging.’ Dental Ultrasound in Periodontology and Implantology. Springer, Cham, 2021. 115-129.
7. Kripfgans, O.D., Chan, HL.(. (2021). Volumetric Ultrasound and Related Dental Applications. In: Chan, HL.(., Kripfgans, O.D. (eds) Dental Ultrasound in Periodontology and Implantology. Springer, Cham. https://doi.org/10.1007/978-3-030-51288-0_12.
8. Chifor, R.; Badea, A. F.; Chifor, I.; Mitrea, D.-A.; Crisan, M.; Badea, M. E., Periodontal evaluation using a non-invasive imaging method (ultrasonography). Med Pharm Rep 2019, 92 (Suppl No 3), S20-S32.
9. Nguyen KCT, Duong DQ, Almeida FT, Major PW, Kaipatur NR, Pham TT, Lou EHM, Noga M, Punithakumar K, Le LH. Alveolar Bone Segmentation in Intraoral Ultrasonographs with Machine Learning. J Dent Res. 2020 Aug;99(9):1054-1061. doi: 10.1177/0022034520920593. Epub 2020 May 11. PMID: 32392449.
10. Izzetti R, Vitali S, Aringhieri G, Oranges T, Dini V, Nisi M, Graziani F, Gabriele M, and Caramella D. Discovering a new anatomy: exploration of oral mucosa with ultra-high frequency ultrasound. Dentomaxillofac Radiol 2020; 49: 20190318.
11. Sinjab, K.; Kripfgans, O. D.; Ou, A.; Chan, H.-L., Ultrasonographic evaluation of edentulous crestal bone topography: A proof-of-principle retrospective study. Oral Surgery, Oral Medicine, Oral Pathology and Oral Radiology 2021.
12. Chifor, R.; Badea, M. E.; Hedesiu, M.; Serbanescu, A.; Badea, A. F., Experimental model for measuring and characterisation of the dento-alveolar system using high frequencies ultrasound techniques. Medical Ultrasonography 2010, 12 (2), 127-32.
13. Nguyen, K. C. T., Le, L. H., Kaipatur, N. R., & Major, P. W. (2016). Imaging the cemento-enamel junction using a 20-MHz ultrasonic transducer. Ultrasound in medicine & biology, 42(1), 333-338.
14. Chan, H.-L.; Wang, H.-L.; Fowlkes, J. B.; Giannobile, W. V.; Kripfgans, O. D., Non-ionizing real-time ultrasonography in implant and oral surgery: A feasibility study. Clinical Oral Implants Research 2017, 28 (3), 341-347.
15. Nguyen, K.-C. T.; Le, B. M.; Li, M.; Almeida, F. T.; Major, P. W.; Kaipatur, N. R.; Lou, E. H. M.; Punithakumar, K.; Le, L. H., Localization of cementoenamel junction in intraoral ultrasonographs with machine learning. Journal of Dentistry 2021, 112, 103752.
16. Pan, Y.-C.; Chan, H.-L.; Kong, X.; Hadjiiski, L. M.; Kripfgans, O. D., Multi-class deep learning segmentation and automated measurements in periodontal sonograms of a porcine model. Dentomaxillofacial Radiology 2021, 50, 20210363.
17. Yi, J.; Nguyen, K.-C. T.; Wang, W.; Yang, W.; Pan, M.; Lou, E.; Major, P. W.; Le, L. H.; Zeng, H., Polyacrylamide/Alginate double-network tough hydrogels for intraoral ultrasound imaging. J. Colloid Interface Sci. 2020, 578, 598-607.
18. Chifor, R.; Li, M.; Nguyen, K.-C. T.; Arsenescu, T.; Chifor, I.; Badea, A. F.; Badea, M. E.; Hotoleanu, M.; Major, P. W.; Le, L. H., Three-dimensional periodontal investigations using a prototype handheld ultrasound scanner with spatial positioning reading sensor. Medical Ultrasonography 2021, 23 (3), 297-304.

19. Chavez, J. P., Wear, K. A., Mantri, Y., Jokerst, J. V., & Vogt, W. C. (2022). Photoacoustic imaging phantoms for assessment of object detectability and boundary buildup artifacts. Photoacoustics, 100348.
20. Slak B, Daabous A, Bednarz W, Strumban E, Maev RG. 2015. Assessment of gingival thickness using an ultrasonic dental system prototype: a comparison to traditional methods. Ann Anat. 199:98–103.
21. Vandana KL, Savitha B. 2005. Thickness of gingiva in association with age, gender and dental arch location. J Clin Periodontol. 32(7):828–830.
22. Matrone, Giulia et al. “Ultrasound plane-wave imaging with delay multiply and sum beamforming and coherent compounding.” 2016 38th Annual International Conference of the IEEE Engineering in Medicine and Biology Society (EMBC) (2016): 3223-3226.
23. Huang, L., Huang, Y., & Gao, K. (2019, March). Transrectal ultrasound imaging using plane-wave, fan-beam and wide-beam ultrasound: Phantom results. In Medical Imaging 2019: Physics of Medical Imaging (Vol. 10948, pp. 911-918). SPIE.
24. D. Q. Le, E. Chang, P. A. Dayton and K. Johnson, ‘High-Framerate Dynamic Contrast-Enhanced Ultrasound Imaging of Rat Kidney Perfusion,’ 2019 IEEE International Ultrasonics Symposium (IUS), 2019, pp. 1326-1329, doi: 10.1109/ULTSYM.2019.8926166.
25. Tavelli L, Barootchi S, Majzoub J, Chan HL, Giannobile WV, Wang HL, Kripfgans OD. Ultrasonographic tissue perfusion analysis at implant and palatal donor sites following soft tissue augmentation: A clinical pilot study. J Clin Periodontol. 2021 Apr;48(4):602-614. doi: 10.1111/jcpe.13424. Epub 2021 Feb 3. PMID: 33465812; PMCID: PMC8058327.
26. https://www.vinno-ultraschall.de/vinno-x10-23l/.
27. Chan H-LA, Kripfgans OD. Ultrasonic Imaging for Evaluating Peri-Implant Diseases. In: Dental Ultrasound in Periodontology and Implantology. Springer; 2021:161-175.
28. Rossmann, K. (1969). Point spread-function, line spread-function, and modulation transfer function: tools for the study of imaging systems. Radiology, 93(2), 257-272.
29. Alexander Ng, MB ChB FRCA MD, Justiaan Swanevelder, MB ChB FRCA FCA(SA) MMed, Resolution in ultrasound imaging, Continuing Education in Anaesthesia Critical Care & Pain, Volume 11, Issue 5, October 2011, Pages 186–192, https://doi.org/10.1093/bjaceaccp/mkr030.
30. http://www.dcconferences.com.au/lcmc2018/pdf/6._Basic_Principles_of_Ultrasound.pdf.
31. Rothlübbers, S., Strohm, H., Eickel, K., Jenne, J., Kuhlen, V., Sinden, D., & Günther, M. (2020, September). Improving image quality of single plane wave ultrasound via deep learning based channel compounding. In 2020 IEEE International Ultrasonics Symposium (IUS) (pp. 1-4). IEEE.

32. Choi, Jim, and Bao Nguyen. “Undefined.” Academic Radiology 4.8 (1997): n. pag. Web.
33. Chen ZY, Zhong JS, Ouyang XY, Zhou SY, Xie Y, Lou XZ. [Gingival thickness assessment of gingival recession teeth]. Beijing Da Xue Xue Bao Yi Xue Ban. 2020 Apr 18;52(2):339-345. Chinese. doi: 10.19723/j.issn.1671-167X.2020.02.023. PMID: 32306020; PMCID: PMC7433469.